

# STRUCTURAL ELUCIDATION OF NEXT GENERATION INHIBITORS OF PROTEIN PHOSPHATASE 5 USING NMR SPECTROSCOPY

Hope P. Hill,\* Noah C. Baker,\* Ivy B. Nguyen,\* and David C. Forbes†

Department of Chemistry, 6040 USA Dr. South, University of South Alabama, Mobile, AL 36608

## Abstract

The overexpression of protein phosphatase 5 (PP5) has been correlated to tumor cell reproduction making it a candidate for small molecule drug therapy. As the selective and potent inhibition of the PP2A domain has been accomplished using a functionalized and decorated scaffold which maximize contacts within and around the active site, an opportunity of inhibition targeting the similar domain of PP5 exists. The naturally occurring inhibitor, cantharidin, has been shown to be a potent yet unselective inhibitor of protein phosphatase. Our hypothesis for selectivity has as a focus derivatives of cantharidin decorated with functionalized attachments in order to affect optimal binding within and around the active site of PP5. As each derivative is prepared synthetically, a unified and programmatic approach toward the assembly and testing of each system is crucial. The key step in our synthetic route involves a Diels-Alder cycloaddition involving functionalized and unfunctionalized dienes and dienophiles. As a mixture of stereoisomers were formed between the robust dienophile *N*-phenylmaleimide and diene furfuryl alcohol (2-(hydroxymethyl)furan), a study on the isomeric elucidation using 2D NMR spectroscopy was conducted and offered key insight onto which isomer to advance.

†corresponding author: dforbes@southalabama.edu

Keywords: NMR spectroscopy, cycloaddition, structural elucidation, drug design

## Introduction

Cantharidin is a naturally occurring inhibitor found in blister beetles and has been used in Chinese medicine for centuries for a wide range of ailments (Figure 1).<sup>1</sup> Recent studies using can-

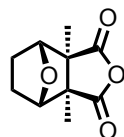
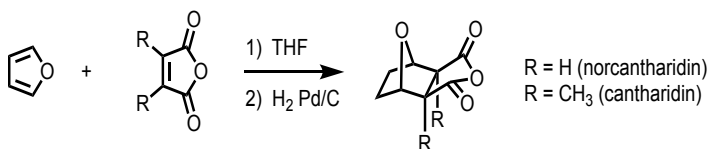


Figure 1. Cantharidin

tharidin and derivatives of cantharidin have shown promise when assayed against serine/threonine protein phosphatases.<sup>2</sup> Within the serine/threonine-family of protein phosphatases, cantharidin has shown particular activity within the domains of PP1CA, PP2CA, PP5C, and PP6C.<sup>3</sup> Notable was the activity found with protein phosphatase 5 (PP5). PP5 is in many protein complexes that contribute to signaling networks that regulate cellular proliferation and apoptosis. An analysis of human breast cancer cells revealed a correlation between the overexpression of PP5 and cancer cell development.<sup>2</sup> Researchers who performed a follow-up study in order to determine if overexpression of PP5 existed, found a direct and positive effect on tumor growth. The experiment compared tumor size development in mice that were injected with differing amounts of PP5 and concluded that PP5 overexpression was directly proportional to tumor size.<sup>2</sup>

Given the interest of cantharidin as a lead compound, research in the development of decorated derivatives of cantharidin has been active. One unique feature when focusing on just its assembly is the efficiency in its preparation when acting on a Diels-Alder cycloaddition. The pericyclic transformation when working with furan and maleic anhydride or 2,3-dimethylmaleic anhydride in one step assembles the core 7-oxabicyclo[2.2.1]heptane scaffold (Scheme 1).

## Scheme 1



When conducted under thermodynamic reaction conditions, the *exo* cycloadduct is exclusively formed and has all four oxygen atoms facially proximal to each other – a feature found to be key when examining binding efficacy in protein phosphatase inhibition (*vide infra*).<sup>3</sup> When approaching the assembly of these systems via a Diels-Alder cycloaddition, another key feature is that both the diene and dienophile can be strategically decorated prior to cycloaddition. This without question offers a viable, extremely attractive, and unified approach toward the assembly of next generation scaffolds.

Co-crystal structures of PP5C and derivatives of cantharidin's demethylated cousin norcantharidin have been published (Figure 2).<sup>3</sup> The key interactions revealed are between the carboxylate oxygens and the bridgehead oxygen of the inhibitor and the

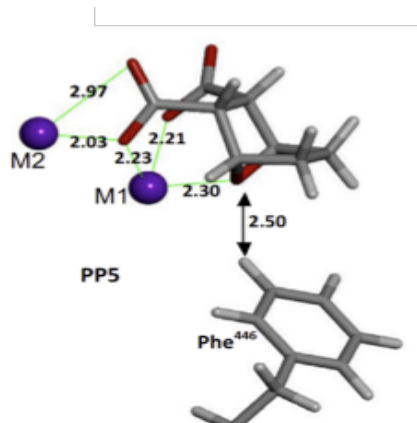


Figure 2. Close-up view of the PP5C complex highlighting interactions between metal ions and the oxygen atoms of endothall which is hydrolyzed norcantharidin.

manganese ions.<sup>4</sup> Closer inspection of the catalytic pocket when docked with a norcantharidin derivative revealed the necessity of close proximity between the oxygen bridgehead of the inhibitor and both the manganese catalytic ions and the amino acid side chain (Phe446) of PP5. Thus, from a structural and retrosynthetic perspective, any synthetic approach employed must advance what would be considered the *exo* isomer when conducting a Diels-Alder cycloaddition. Fortunately for our study, not only does the demethylated analog of cantharidin, norcantharidin, yield the *exo* cycloadduct when working with furan and maleic anhydride, several synthetically prepared norcantharidin derivatives bound at C8 of the core scaffold yield the *exo* cycloadduct exclusively and have shown promise with potential anticancer properties.<sup>5</sup>

With the systems we have prepared and tested to date, our focus has been the assembly of a decorated derivative exhibiting both potency and selectivity. Potent when operating with a bridgehead oxygen in proximity with the anhydride functionality and selective when exploring functionalized derivatives which are tasked to eliminate various negative side effects by increasing favorable contacts within one phosphatase domain over another. Our hypothesis was confirmed when working with a decorated diene consisting of heteroatomic functionality (Chart 1).<sup>3</sup> Starting with not furan but 3-(propoxymethyl)furan, the ether functionality at position C8 resulted in increased inhibition against PP5 while largely deselecting for PP1C. The propoxymethyl group allowed for favorable interaction through supplementary hydrogen bonding with neighboring amino acid residues while still avoiding steric clashes. Steric clashes are believed to be the reason for lower activity of systems with longer groups bound at C8 (e.g. the decoxymethyl group). These results warranted further development of selective and potent inhibitors of PP5.

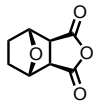
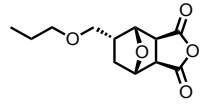
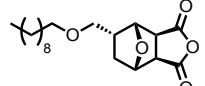
	PP5 IC50	PP1 IC50
	1.0 $\mu\text{M}$	8.9 $\mu\text{M}$
	0.7 $\mu\text{M}$	3.7 $\mu\text{M}$
	14.3 $\mu\text{M}$	21.1 $\mu\text{M}$

Chart 1. Activity and selectivity of norcantharidin against two derivatives.

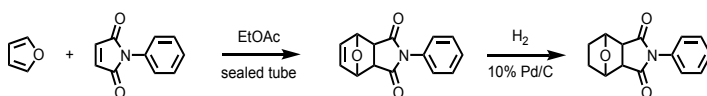
While delighted with the results, a reexamination of our synthetic approach was needed as our overall yields were low and intermediate stability was always a consideration when working with anhydride functionality. The modification we elected to pursue utilized not anhydride functionality but imide functionality as part of the dienophile. The rationale was twofold – the cycloadducts prepared using not anhydride but imide functionality are far more robust and the options we had at our disposal when wanting to transform the imide functionality back to an anhydride were numerous. Given the stability of imide functionality, we felt confident that regardless of where we positioned the sidechain, the resulting cycloadduct would be robust when considering additional synthetic step and/or functional group compatibility.

## Experimental Methods

### General Considerations

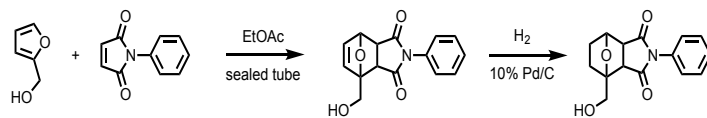
The NMR which generated all the spectra as part of this submission was a JEOL ECA-500 spectrometer. The software used to process all the corresponding data was JEOL Delta™ Version 5.0.4.4 (PC) or 5.2.1 (MAC). <sup>1</sup>H NMR (500 MHz) spectra were obtained as solutions in CDCl<sub>3</sub>. Chemical shifts were reported in parts per million (ppm) and referenced to  $\delta$  7.27 (<sup>1</sup>H NMR). For the synthetic procedures performed, additional considerations consisted of the following: TLC analyses were performed on flexible aluminum backed TLC plates with a fluorescent indicator. Detection was conducted by UV absorption (254 nm) followed by charring with 10% KMnO<sub>4</sub> in water. Solutions were concentrated in vacuo using a rotary evaporator. Crude reaction mixtures were purified using a silica gel column (70-230 mesh, 60 Å). All chemicals used for synthetic procedures were reagent grade or better.

### Diels-Alder Cycloaddition using *N*-Phenylmaleimide and Furan



*N*-Phenylmaleimide (400 mg, 2.31 mmol, 1.0 equiv) was added to a sealed pressure flask equipped with a stir bar and dissolved in 1.6 mL of hot ethyl acetate forming a 1.4 M solution. Furan (252  $\mu\text{L}$ , 3.5 mmol, 1.5 equiv) was next added via syringe once the reaction mixture was allowed to cool back to room temperature. The pressure flask was sealed, placed in a sand bath and externally heated to 100 °C. The reaction was allowed to stir for 16 h. The crude reaction mixture was immediately hydrogenated using 25 mg of 10% Pd/C after transferring the material to a Parr flask and diluted using as a ratio 20 mL of THF per gram of material. The hydrogenation was set at 55 psi and allowed to mix for 1 h after purging the initial blanket of molecular hydrogen three times. After removing the catalyst via filtration using a Celite pad, the product was concentrated under reduced pressure and chromatographed (SiO<sub>2</sub>; EtOAc/hexanes (2:1)). Reaction was replicated on several occasions with yields averaging between quantitative and 95%. <sup>1</sup>H NMR (CDCl<sub>3</sub>)  $\delta$  7.48-7.44 (m, 2H), 7.40-7.37 (m, 1H), 7.27-7.24 (m + CHCl<sub>3</sub>, 2H), 5.00 (dd, 2H, CH,  $J$  = 3.2 Hz,  $J$  = 2.5 Hz), 3.04 (s, 2H, CH) 1.96-1.89 (m, 2H, CH<sub>2</sub>) 1.69-1.65 (m, 2H, CH<sub>2</sub>).

### Diels-Alder Cycloaddition using *N*-Phenylmaleimide and 2-(Hydroxymethyl)furan



2-Furfuryl alcohol (303  $\mu\text{L}$ , 3 mmol, 1.5 equiv) and *N*-phenylmaleimide (400 mg, 2.3 mmol, 1.0 equiv) were added to a sealed pressure flask equipped with a magnetic stir bar and dissolved in ethyl acetate (1.6 mL) to form a 1.4 M solution. The reaction was placed in a sand bath and externally heated to 100 °C. Reaction was allowed to stir for 16 h. The crude reaction mixture was immediately hydrogenated using 25 mg of 10% Pd/C after transferring the material to a Parr flask and diluted using as a ratio 20 mL of THF per gram of material. The hydrogenation was set at 55 psi and allowed to mix for 1 h after purging the initial blanket of molecular hydrogen three times. After removing the catalyst via filtration

using a Celite pad, the product was concentrated under reduced pressure and chromatographed (SiO<sub>2</sub>; EtOAc/hexanes (2:1)). For purposes of determining the isomeric composition, a small portion of chromatographed material was recrystallized (EtOAc with hexanes) resulting in nearly isomerically pure material. Reaction was replicated on several occasions with yields of both the *exo* and *endo* adducts averaging between quantitative and 95% of nearly equal stereochemical composition. Recrystallized product was white powder with a  $R_f = 0.43$  (SiO<sub>2</sub>, EtOAc/hexanes (6:1)). The more polar isomer had a  $R_f = 0.55$  (SiO<sub>2</sub>, EtOAc/hexanes (6:1)). While we were unsuccessful in chromatographically separating the isomers, we were able to obtain enriched material of adequate purity and the spectral data below corresponds to the more polar, lower  $R_f$  material. <sup>1</sup>H NMR (CDCl<sub>3</sub>)  $\delta$  7.50-7.46 (m, 2H, CH), 7.43-7.39 (m, 1H, CH), 7.28-7.25 (m, 2H + CHCl<sub>3</sub>, CH), 5.01 (d, 1H, CH,  $J = 5.5$  Hz), 4.07 (dd, 2H, CH<sub>2</sub>,  $J = 12.5$  Hz), 3.21-3.17 (m, 2H, CH), 2.10-2.02 (m, 1H, CH), 1.92-1.87 (m, 2H, CH), 1.81-1.76 (m, 1H, CH). The diagnostic peak of the less polar, higher  $R_f$  material is the following:  $\delta$  4.98 (t, 1H, CH,  $J = 5.0$  Hz).

## Results and Discussion

Knowing that downstream synthetic steps may compromise the anhydride functionality when working with maleic anhydride as dienophile, *N*-phenylmaleimide was seen as a suitable alternative. Furthermore and by design de novo, use of *N*-phenylmaleimide addressed prior obstacles of product isolation and reaction monitoring having confidence that the imide could be transformed in a final synthetic step restoring the anhydride, functionality that has been shown to be key in inhibition of PP5.<sup>6</sup>

As we did with the prior series, we started with a model system involving furan and *N*-phenylmaleimide. Using this diene and dienophile respectively, the desired cycloadduct was isolated in high yield. While the *exo* isomer would be considered the thermodynamically favored cycloadduct, this had yet to be confirmed especially when working with maleimide derivatives. Furthermore, without crystals suitable for x-ray analysis, we resorted to NMR spectroscopy for stereochemical assignments and felt confident that for our model system, one stereoisomer predominated based upon the two diagnostic peaks at  $\delta$  5.00 (H<sub>1</sub>, H<sub>7</sub>) and  $\delta$  3.04 (H<sub>2</sub>, H<sub>6</sub>) (Chart 2).

However, under replicated reaction conditions both the *endo* and *exo* cycloadducts based upon NMR analysis of the crude reaction mixture were observed when replacing furan with 2-(hydroxymethyl)furan (Chart 3).

The isomers when working with the diene 2-(hydroxymethyl)furan, interestingly, could not be identified by the signal splitting patterns and as detailed above, the model system used to confirm either stereoisomer, exclusive nor enriched, did not align with the spectra generated.<sup>7</sup>

We were not discouraged as structural information using NMR spectroscopy was still possible given that the spin-spin coupling denoted by splitting patterns alone was not able to reveal which protons were giving rise to the coupling displayed in individual peaks. That is, to garner more information on positioning of the diagnostic protons, our focus became bond correlations and as such, we resorted to the two-dimensional NMR spectroscopic technique COSY.<sup>8,9</sup>

Our thought process was the following: Given the rigidity of the norcantharidin derivative and the relative stereochemical positioning of the diagnostic protons – both would be directly revealed through the correlations or perhaps more importantly, lack of correlations displayed by the two-dimensional NMR spectra when comparing the two cycloadducts. Crucial with this study is the fact that only upon isolation/enrichment of both stereoisomers and subjecting each to two-dimensional NMR analysis were we able to assign relative configurations (*endo* vs *exo* cycloadduct) (Charts 4 & 5).

As highlighted in Chart 4, there is a clear cross peak correlation when focusing on the peaks representing positions 6 and 7 of the less polar material identified in the crude reaction mixture. Chart 5 offers evidence that a cross peak correlation does not exist with the peaks representing positions 6 and 7.

Even with evidence (and the lack of evidence) of cross peak correlations, supplemental data was necessary to confirm our stereochemical assignments using the two-dimensional NMR technique COSY. We elected to use two independent sources which consisted of the coupling constants of first camphor and second, the dihedral bond angles generated from Spartan software<sup>10</sup> of both

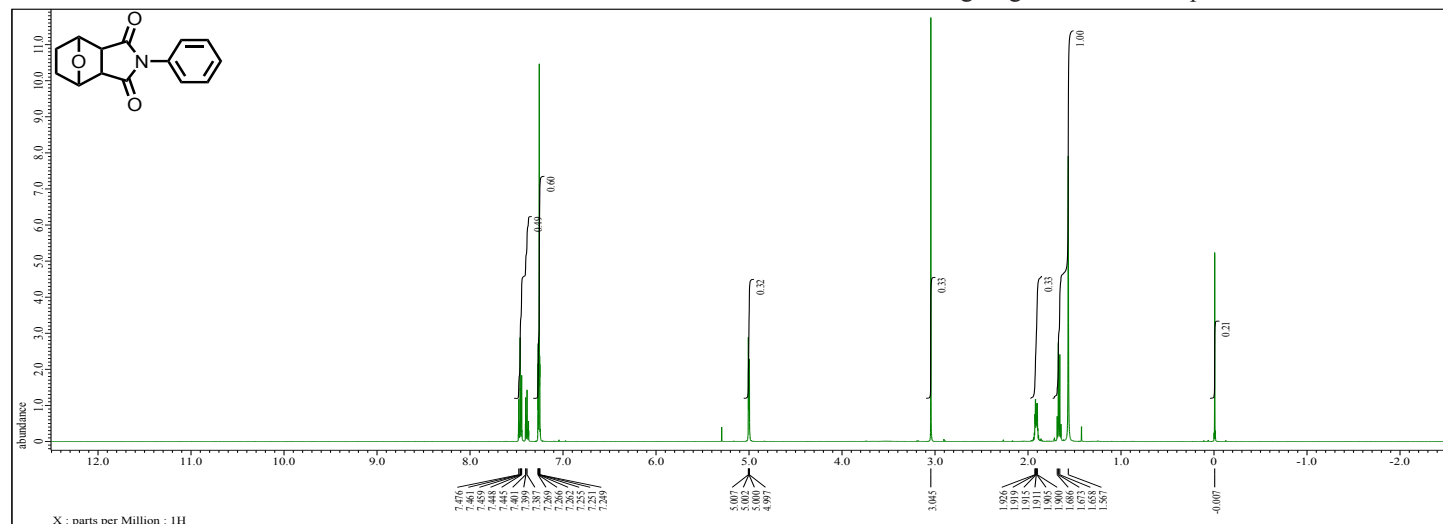


Chart 2. NMR spectrum of crude reaction mixture when reacting furan with *N*-phenylmaleimide.

the *endo* and *exo* cycloadducts. For the former, we were able to validate our analysis using the effects of bond angle on the coupling constant  $J$  between the protons  $H_a$ -C-C- $H_b$  of camphor where  $H_a$  represents  $H_1$  and  $H_b$  represented either the *exo*-C-H position ( $H_{6x}$ ) or that of  $H_{6n}$  (Figure 3).<sup>11</sup>

For situations where the Newman projection has the dihedral an-

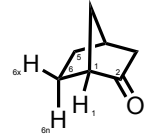
	dihedral angle	observed coupling	
	$H_{6x}$ -C-C- $H_1$	$77.26^\circ$	0.1 Hz
	$H_{6n}$ -C-C- $H_1$	$44.91^\circ$	4.7 Hz

Figure 3. Camphor

gle between  $H_a$  and  $H_b$  approaching  $90^\circ$ , the coupling constant approaches 0 Hz. Conversely, as the bond angle approaches  $0^\circ$  or  $180^\circ$ , the larger the coupling constant becomes. When focusing on camphor, a bicyclic[2.2.1]scaffold which mimics our cycloadduct, the dihedral bond angle for  $H_{6n}$ -C-C- $H_1$  is  $44.91^\circ$  and the coupling is 4.7 Hz. Switching from the *endo* to the *exo* proton, the  $H_{6x}$ -C-C- $H_1$  bond angle is  $77.26^\circ$  resulting in an observed value of 0.1 Hz.<sup>9</sup>

Our second independent source focused on the dihedral bond angles using both the *endo* and *exo* cycloadducts and were derived using Spartan software. We were very pleased to see the similarity between the prior system of camphor highlighting the proton at the bridgehead carbon and the adjacent methylene and the presence and absence of cross peak correlations (Charts 4 & 5). For the Spartan software analysis, we were honing in on the proton of the bridgehead carbon and that of the adjacent methine. The dihedral bond angles generated provide a direct correlation to the COSY spectra generated having established the coupling constants of camphor and very similar assignments. A unified comparison of the data generated is below in Figure 4.

For the synthesized Diels-Alder adducts using 2-(hydroxymethyl)furan, the dihedral bond angle, as determined by Spartan, of  $H_{6x}$ -C-C- $H_7$  (the *endo* adduct) is  $36.23^\circ$  while the dihedral bond angle of  $H_{6n}$ -C-C- $H_7$  (the *exo* adduct) is  $81.91^\circ$ . Therefore, positioned hydrogen  $H_{6x}$  of what now we can assign as the *endo*-Diels-Alder adduct correlates with both Chart 4 and the less polar material. For the positioned hydrogen  $H_{6n}$ , the stereoisomer can now be assigned as the *exo*-Diels-Alder adduct which offers no cross correlation as illustrated in Chart 5 and corresponds to the more polar cycloadduct. For both systems, it is the dihedral angles calculated and confirmed using the cross correlations with the bridgehead proton ( $H_7$ ).<sup>10</sup> Furthermore, the presence and absence of the coupling is indeed reflected in the given correlations of the respective COSY NMR spectra from which it can be deduced that the observed triplet places  $H_6$  in the *exo* position of the *endo*-Diels-Alder adduct and coupled to both  $H_{2x}$  and  $H_7$  (Figure 4). Likewise, the observed doublet is a result where coupling is not apparent with the bridgehead proton ( $H_7$ ) and thus places  $H_6$  in the *endo* position of the *exo*-Diels-Alder adduct and coupled to only  $H_{2n}$ .

And finally, when circling back to the cycloadduct generated when working with furan and *N*-phenylmaleimide, the COSY generated interestingly does not confirm cross peak correlations for protons at positions 1/7 and 2/6 (Chart 6) hence we can conclude

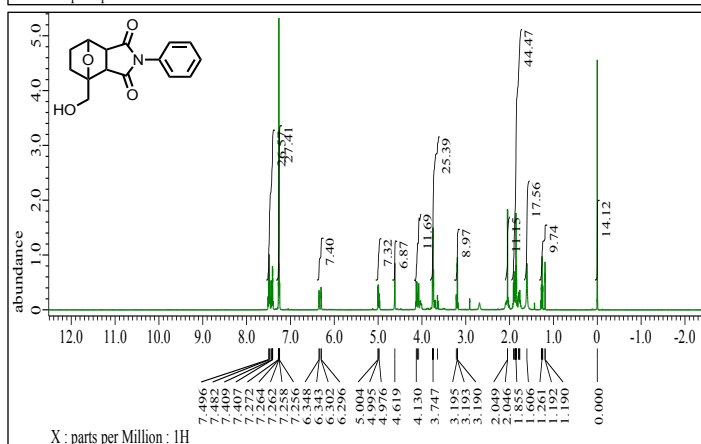
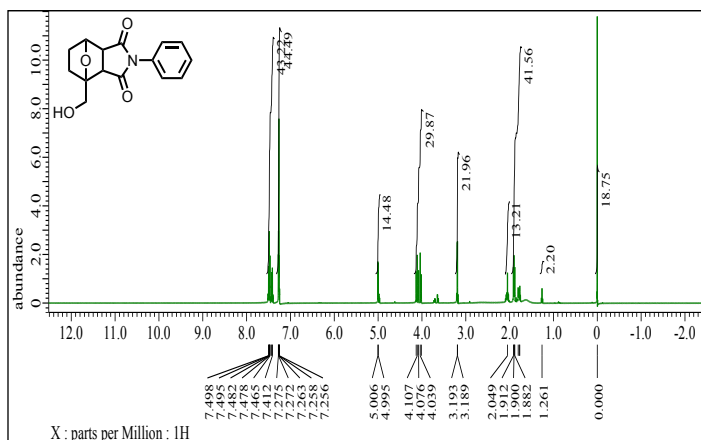


Chart 3. NMR spectra of both recrystallized material (top spectrum) and crude reaction mixture (bottom spectrum) of cycloadducts when reacting 2-(hydroxymethyl)furan with *N*-phenylmaleimide.

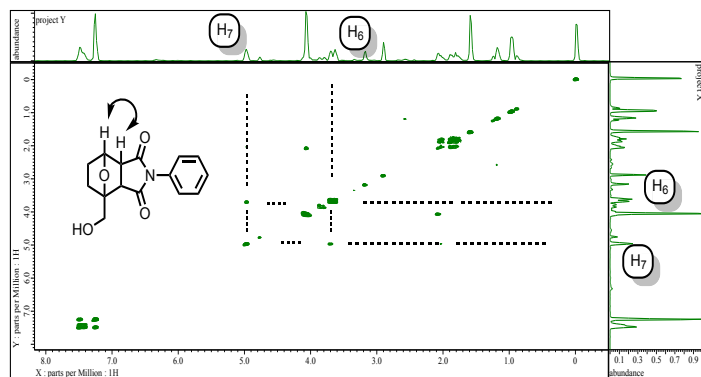


Chart 4. COSY of less polar cycloadduct confirming cross peak correlations when focusing on positions 6 and 7.

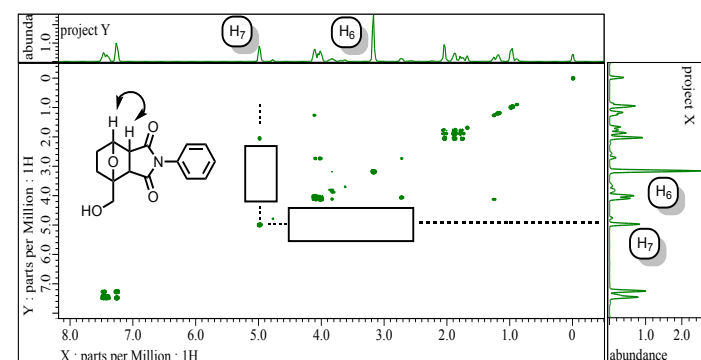
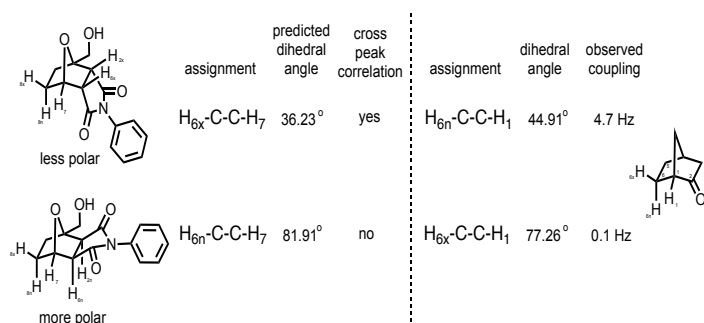
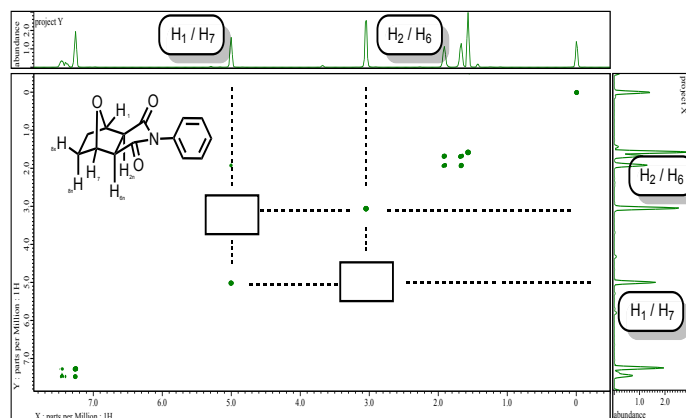


Chart 5. COSY of more polar and recrystallized cycloadduct not having cross peak correlations when focusing on positions 6 and 7.



**Figure 4.** A comparison of the data generated with the cross peak correlations using two independent sources confirming the presence or absence of coupling.



**Chart 6.** COSY of cycloadduct using furan and *N*-phenylmaleimide not having cross peak correlations when focusing on positions 1/2n and 6n/7.

that for this system, it is the *exo* cycloadduct which is supported by the doublet of doublets observed for the bridgehead proton. Furthermore and perhaps more interestingly, the disconnect between bond correlations and spin-spin coupling denoted by splitting patterns is evident in this system. While a cross peak correlation is not observed with the protons bound to positions 1/7 and 2/6, spin-spin coupling denoted by splitting patterns is apparent when examining the peak at 5.00 ppm which is observed as a doublet of doublets because of the adjacent methylene. While it would be best to have a mixture and duplicate what was done above when working with 2-(hydroxymethyl)furan, the data, especially that of the COSY, does support an *exo* cycloadduct.

## Conclusion

Replacement of anhydride functionality with imide resulted in the formation of isomers upon reaction of 2-hydroxymethylfuran and *N*-phenylmaleimide. While prior work established absolute and relative assignments because crystals suitable for x-ray analysis were obtained, insight into which cycloadduct was generated using *N*-phenylmaleimide was possible using two-dimensional NMR spectroscopy. The two-dimensional NMR technique COSY gave diagnostic correlations between the protons on positions 6 and 7 of each cycloadduct. Only with the generation of both stereoisomers, use of supplemental data, and having success with the enrichment/isolation of each were we able to confirm relative stereochemical assignments. Success in confirming and enriching the more polar *exo* cycloadduct will allow for the assembly of the proper next generation system earmarked toward a potent and selective inhibitor of PP5 using the more robust dienophile *N*-phenylmaleimide.

## Acknowledgements

Support from the Department of Chemistry, University Honors College, and University of South Alabama Foundation is gratefully acknowledged.

## References

- Wang, G., Dong, J., & Deng, L. (2018). Overview of Cantharidin and Its Analogues. *Current Medicinal Chemistry*, 25, 2034–2044.
- Golden, T., Aragon, I. V., Rutland, B., Tucker, J. A., Shevde, L. A., Samant, R. S., Zhou, G., Amable, L., Skarra, D., and Honkanen, R. E. (2008) Elevated Levels of Ser/Thr Protein Phosphatase 5 (PP5) in Human Breast Cancer. *Biochimica et Biophysica Acta (BBA) - Molecular Basis of Disease* 1782, 259–270.
- Chattopadhyay, D., Swingle, M. R., Salter, E. A., Wood, E., D'Arcy, B., Zivanov, C. N., Abney, K., Musiyenko, A., Rusin, S. F., Kettenbach, A., Yet, L., Schroeder, C. E., Golden, J. E., Dunham, W. H., Gingras, A. C., Banerjee, S., Forbes, D. C., Wierzbicki, A., Honkanen, R. E. (2016). Crystal Structures and Mutagenesis of PPP-family Ser/Thr Protein Phosphatases Elucidate the Selectivity of Cantharidin and Novel Norcantharidin- Based Inhibitors of PP5C. *Biochemical Pharmacol.*, 109, 14–26.
- Bertini, I., Calderone, V., Fragai, M., Luchinat, C., and Talluri, E. (2009) Structural Basis of Serine/Threonine Phosphatase Inhibition by the Archetypal Small Molecules Cantharidin and Norcantharidin. *J. Med. Chem.* 52, 4838–4843.
- Hill, T. A., Stewart, S. G., Gordon, C. P., Ackland, S. P., Gilbert, J., Sauer, B., Sakoff, J. A., and McCluskey, A. (2008) Norcantharidin Analogues: Synthesis, Anticancer Activity and Protein Phosphatase 1 and 2A Inhibition. *ChemMedChem* 3, 1878–1892.
- Bertini, I., Calderone, V., Fragai, M., Luchinat, C., and Talluri, E. (2009) Structural Basis of Serine/Threonine Phosphatase Inhibition by the Archetypal Small Molecules Cantharidin and Norcantharidin. *J. Med. Chem.* 52, 4838–4843.
- Uemura, N., Toyoda, S., Ishikawa, H., Yoshida, Y., Mino, T., Kasashima, Y., & Sakamoto, M. (2018). Asymmetric Diels–Alder reaction involving Dynamic Enantioselective Crystallization. *The Journal of Organic Chemistry*, 83(16), 9300–9304.
- The popular 2D NMR technique, homonuclear correlation spectroscopy or COSY, reveals homonuclear through bond correlations. If the nuclei of protons have interaction and therefore display coupling, it is denoted by cross peak correlations. The resulting COSY graph displays the one-dimensional NMR on both the x and y axis. Plot points appear where a correlation exists; each peak will be correlated to itself resulting in a series of linear points whereas nonlinear points display correlations between protons of differing chemical shifts. These nonlinear points reveal which protons are connected to one another through bond. Therefore, combining the data of one-dimensional and two-dimensional NMR spectroscopy gives both structural and connectivity information.
- Simpson, J. H. (2008). *Organic Structure Determination using 2-D NMR Spectroscopy: A Problem-Based Approach*. 117–118.
- Spartan 14v112 (2013) Wavefunction, Inc., Irvine, CA

11. Ernő, P. and & Biemann, K. (1989). *Tables of Spectral Data for Structure Determination of Organic Compounds*. Springer Verlag.